Multiband description of the optical properties of zincblende nitride quantum dots

Stefan Schulz,[1] Daniel Mourad,[2] and Gerd Czycholl[2]
[1]*Tyndall National Institute, Lee Maltings, Cork, Ireland*
[2]*Institute for Theoretical Physics, University of Bremen, 28359 Bremen, Germany*
(Received 5 June 2009; revised manuscript received 5 August 2009; published 8 October 2009)

We use the single-particle energies and wave functions calculated from an effective bond-orbital model and a microscopic empirical tight-binding model in combination with the configuration-interaction scheme to calculate the optical properties of cubic GaN/AlN quantum dots. Special attention is paid to the possible influence of the weak spin-orbit coupling on the optical spectra. The results are compared to recent experimental data. In agreement with the experiments, we find a strong polarization anisotropy of the excitonic transitions in the microscopic empirical tight-binding model, while the effective bond-orbital model misses this anisotropy in the absence of a piezoelectric field and an atomistic strain field. This missing anisotropy can be attributed to the artificially increased symmetry of the combined system of quantum dot geometry and underlying lattice structure.

DOI: 10.1103/PhysRevB.80.165405 PACS number(s): 78.67.Hc, 73.22.Dj, 71.35.−y

I. INTRODUCTION

Wide band gap GaN, among other group-III–nitride-based semiconductors, have been successfully employed to realize short-wavelength light-emitting diodes and laser diodes.[1] Additionally, owing to quantum confinement effects, fabrication and studies of GaN-based quantum dots (QDs) have recently attracted a great deal of interest for potential applications in electronic and optoelectronic devices due to their unique physical properties.[2,3] For instance, the application of QD structures in laser diodes has been known to lead to lower threshold currents due to the enhancement of excitonic effects in low-dimensional systems.[4] Despite their potential for optoelectronic applications, the electronic and optical properties of group-III–nitride QDs are still far less known than those of the more traditional III-V-semiconductor QD systems.

Self-assembled GaN QDs have been grown mainly in the hexagonal phase. In comparison to conventional III-V materials, the wurtzite group-III nitrides exhibit very strong electrostatic built-in fields.[5–7] These fields arise in part from spontaneous and in part from strain-induced polarizations and as a consequence, the optical properties of nitride-based nanostructures are significantly modified by these contributions. For instance, the built-in field gives rise to a strong separation of electron and hole wave functions.[8,9] Consequently, the optical recombination rate in these structures is drastically reduced.

To overcome these problems, there has been a rapid increase in the studies of nitride-based QD structures grown along nonpolar directions.[10–12] The experimental data on these systems indicate that the polarization effects can in fact be reduced.[10] However, recent theoretical results also indicate that the growth of nonpolar QDs will still lead to residual built-in fields.[13] Clearly, these fields will need to be considered when constructing optoelectronic devices.

As discussed in detail by Simon *et al.*[6] and Novikov *et al.*,[7] the direct way to eliminate the built-in field across the QD structure is to grow zincblende III–nitride-based QDs along the *non*polar [001] direction. Since these structures offer many potential advantages over systems grown in the wurtzite phase, the interest in nitride-based nanostructures with a zincblende structure is now strongly increasing. Some of the advantages are the absence of the strong electrostatic built-in field across the nanostructure, the higher carrier mobility due to the higher crystallographic symmetry of the system,[7,14] the possibility to cleave (100) zincblende systems on the {110} plane, which is especially interesting for device applications,[7,15] and the smaller energy gap in cubic GaN compared to the wurtzite system, which reduces the required indium content to obtain green light emission.[14] High-quality self-assembled zincblende GaN/AlN QDs have now been demonstrated and experimentally investigated.[6,16–20]

In order to investigate the optical properties of these nanostructures, the single-particle states and energies are of crucial importance. Therefore, we compare in a first step the electronic structure of the nanostructure under consideration calculated from an effective bond-orbital model to those of a microscopic empirical tight-binding approach. Since we use the same set of input parameters, the results can be directly compared. However, the single-particle states and energies themselves are not observed in the optical measurements. In the experiments, the optical properties of self-assembled semiconductor QDs are often analyzed a function of the excitation power and therefore as a function of the number of electrons and holes in the system.[21] To calculate the optical spectra of these structures, one has to deal with a system of a few charge carriers in the discrete states of a given confinement potential, where the carriers interact via the Coulomb interaction. To address this problem, different theoretical approaches have been proposed to study the optical properties of self-assembled QDs, e.g., the Hartree-Fock method[22] and the configuration-interaction (CI) scheme.[22,23] The latter approach uses the single-particle wave functions of the QD system to construct the many-particle states.

In this paper, we use the approach presented in Ref. 8 to combine the single-particle multiband wave functions with CI calculations for the evaluation of the many-body states. Since the multiband approaches are using the same set of input parameters and the Coulomb interaction is treated in the same way, we are able to compare the results obtained for

the optical properties of a model QD using the above mentioned slightly different approaches. Furthermore, the results can also be compared to recent experimental data[24] as fingerprints of the electronic structure of QDs. Additionally, we will pay special attention to the possible influence of the weak spin-orbit coupling on the optical properties, as this contribution is often neglected in calculations for nitride-based QDs.[8,9,25–29]

This paper is organized as follows. In Sec. II, we introduce the main ingredients of our theory for the calculation of the electronic and optical properties of GaN QDs with a zincblende structure. These ingredients include the microscopic empirical tight-binding model, an effective bond-orbital approach, and the evaluation of Coulomb and dipole matrix elements from the calculated single-particle states. Section III A deals with the electronic structure of GaN/AlN QDs, while Sec. III B is dedicated to the excitonic absorption spectrum and the polarization anisotropy of these systems.

II. THEORY

For a proper treatment of the single-particle states and energies and therefore the optical properties of semiconductor QDs, a multiband approach is required.[30] To study the influence of the atomistic structure of the underlying lattice, we choose here two different models, namely, the effective bond-orbital model (EBOM) and a microscopic empirical tight-binding model (ETBM). The general aspects of these approaches are discussed in detail in Refs. 31 and 32. For the calculation of Coulomb and dipole matrix elements, we follow here the guidelines given in Ref. 8. We briefly summarize the main ingredients of the subsequently used approaches in Secs. II A and II B, while Sec. II C introduces the model QD geometry and deals with the implementation of the EBOM and ETBM for semiconductor QDs. Section II D is dedicated to the many-body Hamiltonian for a system of interacting charge carriers.

A. ETBM

The empirical tight-binding approach enables an atomistic treatment of a nanostructure, since each site of the underlying lattice is described by a certain number of localized atomic orbitals. Such an approach provides a simple physical picture in terms of atomic orbitals and on-site as well as interatomic matrix elements between these orbitals. Due to the strong localization of the orbitals at the atomic sites, a cutoff after a few neighboring shells is well justified.

Here, we apply a tight-binding (TB) model with a $s_c p_a^3$ basis set, which implies that each anion is described by three p orbitals per spin direction while the cation is modeled by a single s orbital per spin direction. The coupling of the basis states is restricted to nearest and second-nearest neighbors. Spin-orbit coupling is taken into account according to Ref. 33. By analytic diagonalization of the bulk TB Hamiltonian for selected $\mathbf{k}$ directions, the electronic dispersion is obtained as a function of the different TB parameters. Equations for the TB parameters can be deduced as a function of the Kohn-Luttinger parameters $(\gamma_1, \gamma_2, \gamma_3)$, the effective electron mass m_e, the energy gap E_g, and the spin-orbit coupling Δ_{so} at the Brillouin-zone center. If not indicated otherwise, all parameters are taken from Ref. 32. In the framework of this approach, one TB parameter has to be determined self-consistently to reproduce the L-point energy of the split-off valence band. Within this scheme, the band structure around the Γ point is described accurately. The resulting band structure for GaN is shown in Ref. 32.

B. EBOM

In contrast to the microscopic ETBM approach, the effective bond-orbital model neglects the atomic basis of the underlying crystal structure. Therefore, in the case of a zincblende system, the EBOM is based on an effective face-centered cubic (fcc) lattice, i.e., each anion-cation pair in a zincblende lattice is treated as a single lattice site. Thus, the symmetry of the bulk system is changed from T_d (zincblende) to O_h (fcc) and the atomic orbitals are replaced by effective molecular orbitals.

In the framework of the EBOM approach with coupling up to second-nearest neighbors, the required TB-matrix elements can be directly related to the input parameters of the corresponding $\mathbf{k}\cdot\mathbf{p}$ Hamiltonian.[34] Therefore, a self-consistent fitting procedure is not necessary and the EBOM matrix elements can be directly calculated from the Kohn-Luttinger parameters, electron effective mass around the Γ point, etc. By using the parametrization of Ref. 34, the EBOM approach has another advantage over the $s_c p_a^3$ ETBM presented above. In contrast to the $s_c p_a^3$ ETBM, the applied EBOM allows for the reproduction of the X-point energies of the conduction band (X_1^c) as well as the light-hole/heavy-hole (X_3^v) and split-off energies (X_5^v). The resulting band structure from this approach is shown and compared to the ETBM band structure in detail in Ref. 32. Here, we will briefly summarize the results.

The EBOM reproduces the bulk valence-band structures of the materials under consideration throughout the first Brillouin zone. The ETBM band structure is in very good agreement with the EBOM results along the Γ-L direction, while slight differences can be observed near the X point. Furthermore, since the EBOM is designed to reproduce the conduction-band energy at the X point, the EBOM conduction band exhibits an additional maximum along the Γ-X direction. This maximum is in excellent agreement with results from *ab initio* band-structure calculations.[35] The ETBM conduction-band structure misses this additional feature since higher conduction bands are not taken into account. However, since we are dealing with a nanostructure formed from a direct-band gap material here, the Brillouin-zone center is expected to dominate the single-particle states and energies of the QD. Additionally, owing to the large energetic separation between the Γ point and the X and L points, the mixing between these states due to quantum confinement effects is expected to be of minor importance. Indeed, as we will show later, the calculated single-particle states and energies from the EBOM and the $s_c p_a^3$ ETBM are in very good agreement. Therefore, we conclude that the Brillouin-zone center dominates the single-particle states in GaN/AlN QDs.

C. Model GaN quantum dot

High-quality self-assembled zincblende GaN/AlN QDs have been made available recently.[6,16–20] Atomic force microscopy[16] and high-resolution electron microscopy[18] indicate that these nanostructures are grown as truncated pyramids, nucleating on a wetting layer. Furthermore, these studies reveal almost no intermixing between Ga and Al in these structures. Therefore, we assume as a model QD structure a truncated pyramid of pure GaN with a base length of $b=7$ nm and a height of $h\approx 1.75$ nm oriented along the [001] direction and embedded in a pure AlN matrix. The nanostructure resides on a GaN wetting layer with a thickness of $h_{\mathrm{wl}}\approx 0.22$ nm. A more detailed discussion of the QD geometry in comparison to the experimental data is given in Ref. 32.

To calculate the electronic structure of the QD under consideration, a sufficiently large supercell is chosen to avoid numerical artifacts of the supercell boundaries on the bound single-particle states. The convergence of the eigenstates with respect to the supercell has been carefully verified.

In the framework of the $s_c p_a^3$ ETBM, the QD is modeled on an atomistic level. Therefore, the C_{2v} symmetry of the underlying zincblende structure is naturally included in this approach. The parameters for each site are set according to the occupying atoms (Ga, Al, N) in the GaN/AlN heterostructure. At the GaN/AlN interfaces, averages of the TB parameters are used to take into account that the nitrogen atoms cannot unambiguously be attributed to the GaN or AlN material, respectively. The valence-band offset ΔE_v between GaN and AlN is included in our model by shifting the diagonal matrix elements of the bulk GaN.

The description of the nanostructure in the EBOM approach is very similar to the ETBM ansatz. The main difference here is the use of a slightly more coarse-grained grid where the anion and cation structure of the underlying zincblende lattice is not resolved. Therefore, we are left with a fcc lattice instead of a zincblende structure. Doing so, the symmetry of the combined system of QD structure plus underlying lattice is changed from C_{2v} to C_{4v}.

Furthermore, since the EBOM does not resolve the atomistic structure, the spatial resolution of the confinement potential in the EBOM will be slightly different compared to the ETBM approach. To take this effect properly into account, we shift the QD boundaries by half a lattice constant inwards. Doing so, the EBOM and the ETBM results for the single-particle energies are in very good agreement as we will discuss in Sec. III A. From this we can conclude that the confinement potential introduced in the EBOM is fairly close to the confinement potential introduced by the ETBM.

Here, our main focus is on a detailed comparison of the ETBM and the EBOM approaches and the resulting optical properties of a GaN/AlN QD rather than describing the nanostructure in all details. Therefore, to investigate the inherent properties of these approaches, we neglect the contributions of strain and piezoelectricity. Nevertheless, as discussed in detail in Ref. 32, the results for the one-particle level structure are in qualitative agreement with results obtained in Ref. 25, where strain and piezoelectricity are explicitly taken into account.

D. Many-body Hamiltonian, Coulomb, and dipole matrix elements

From the calculated single-particle states, the many-body Hamiltonian H can be constructed

$$H = H_0 + H_C + H_D,$$

$$\text{where} \quad H_0 = \sum_i \epsilon_i^e e_i^\dagger e_i + \sum_i \epsilon_i^h h_i^\dagger h_i \tag{1}$$

is the one-particle part, which is diagonal with respect to the calculated QD eigenstates,

$$H_C = \frac{1}{2}\sum_{ijkl} V_{ij,kl}^{ee} e_i^\dagger e_j^\dagger e_k e_l + \frac{1}{2}\sum_{ijkl} V_{ij,kl}^{hh} h_i^\dagger h_j^\dagger h_k h_l - \sum_{ijkl} V_{ij,kl}^{he} h_i^\dagger e_j^\dagger e_k h_l$$

describes the Coulomb interaction between the carriers, and

$$H_D = \sum_{i,j} (\langle \psi_i^e | e_0 \mathbf{E}\mathbf{r} | \psi_j^h \rangle e_i h_j + \text{H.c.}) \tag{2}$$

denotes the coupling to an external field $\mathbf{E}$ in dipole approximation, where e_0 denotes the bare electron charge. The creation and annihilation operators for electrons (holes) in the single-particle state $|\psi_i^e\rangle$ ($|\psi_i^h\rangle$) with energy $\epsilon_i^e(\epsilon_i^h)$ are denoted by $e_i^\dagger(h_i^\dagger)$ and $e_i(h_i)$, respectively. The Coulomb matrix elements are denoted by $V_{ijkl}^{\lambda,\lambda'}$. According to the discussion of Ref. 8, the $V_{ijkl}^{\lambda,\lambda'}$ are approximated by

$$V_{ijkl}^{\lambda,\lambda'} = \sum_{\substack{\mathbf{R}\\ \mathbf{R}'}} \sum_{\substack{\alpha\beta\\ \sigma\sigma'}} c_{\mathbf{R},\alpha,\sigma}^{\lambda,i*} c_{\mathbf{R}',\beta,\sigma'}^{\lambda',j,*} c_{\mathbf{R}',\beta,\sigma'}^{\lambda',k} c_{\mathbf{R},\alpha,\sigma}^{\lambda,l} V(\mathbf{R}-\mathbf{R}'), \tag{3}$$

with

$$V(\mathbf{R}-\mathbf{R}') = \frac{e_0^2}{4\pi\varepsilon_0\varepsilon_r|\mathbf{R}-\mathbf{R}'|} \quad \text{for} \quad \mathbf{R}\neq\mathbf{R}' \tag{4}$$

and

$$V(0) = \frac{1}{V_{uc}^2}\int_{uc} d^3r d^3r' \frac{e_0^2}{4\pi\varepsilon_0\varepsilon_r|\mathbf{r}-\mathbf{r}'|} \approx V_0. \tag{5}$$

Here, the atomic positions are denoted by $\mathbf{R}$. The calculation of the on-site integral $V(0)$ involves the integration over the volume of the unit cell V_{uc} and can be done quasianalytically by expansion of the Coulomb interaction in terms of spherical harmonics.[36] The expansion coefficients $c_{\mathbf{R},\alpha,\sigma}^i$ are related to the ith one-particle wave function

$$\psi_i(\mathbf{r}) = \sum_{\mathbf{R},\alpha,\sigma} c_{\mathbf{R},\alpha,\sigma}^i \phi_{\mathbf{R},\alpha,\sigma}(\mathbf{r}), \tag{6}$$

where $\phi_{\alpha,\mathbf{R}\sigma}(\mathbf{r})$ denotes the atomic wave functions localized at the lattice site $\mathbf{R}$, i.e., $\alpha\in\{s,p_x,p_y,p_z\}$ and $\sigma\in\{\uparrow,\downarrow\}$, for a multiband approach taking spin-orbit coupling into account.

In addition to the Coulomb matrix elements, one has to calculate the matrix elements $\mathbf{d}_{ij}^{eh}=e_0\langle\psi_i^e|\mathbf{r}|\psi_j^h\rangle$ of the dipole operator $e_0\mathbf{r}$ using the ETBM and EBOM wave functions $\psi_i(\mathbf{r})$, respectively. This expression gives information on the

selection rules, allowed and forbidden transitions, and oscillator strengths.[37] For the operator $\mathbf{r}$ in the dipole Hamiltonian, Eq. (2), we use the approximation[37–39]

$$\mathbf{r} = \sum_{\substack{\mathbf{R} \\ \alpha\sigma}} |\mathbf{R},\alpha,\sigma\rangle \mathbf{R} \langle \mathbf{R},\alpha,\sigma| + \sum_{\substack{\mathbf{R} \\ \alpha\sigma}} \sum_{\substack{\mathbf{R}' \\ \beta\sigma'}} |\mathbf{R},\alpha,\sigma\rangle\langle \mathbf{R},\alpha,\sigma|\tilde{\mathbf{r}}|\mathbf{R}',\beta,\sigma'\rangle\langle \mathbf{R}',\beta,\sigma'|, \quad (7)$$

where $\tilde{\mathbf{r}}$ denotes the position inside a unit cell relative to $\mathbf{R}$. With this decomposition of the operator $\mathbf{r}$ and the single-particle wave functions, Eq. (6), the dipole matrix elements $d_{ij}^{eh} = \mathbf{e}\mathbf{d}_{ij}^{eh}$ explicitly read

$$d_{ij}^{eh} = e_0 \sum_{\substack{\mathbf{R}\mathbf{R}' \\ \alpha\beta\sigma\sigma'}} c_{\mathbf{R},\alpha,\sigma}^{i,e*} c_{\mathbf{R}',\beta,\sigma'}^{j,h} \cdot [\mathbf{e}\mathbf{R}\delta_{\mathbf{R}\mathbf{R}'}\delta_{\alpha\beta}\delta_{\sigma\sigma'} + \langle \mathbf{R},\alpha,\sigma|\mathbf{e}\mathbf{r}|\mathbf{R}',\beta,\sigma'\rangle], \quad (8)$$

where $\mathbf{e}$ denotes the light polarization vector.

The first part in Eq. (8) stems from the expansion coefficients ("envelope") weighted with the position of the corresponding atom site. The second part contains the matrix elements of the operator $\mathbf{r}$ with the localized (atomic) basis orbitals $\phi_{\alpha\mathbf{R}}(\mathbf{r})$ and is determined by their spatial dependence inside the unit cell. Following the discussion of Ref. 8, this orbital part must be calculated using orthogonalized Slater orbitals. In order to estimate the importance of the orbital part, we performed the calculation for different light polarizations. It turned out that the orbital part, for light polarizations parallel to $[110]$, $[1\bar{1}0]$, and $[001]$, respectively, is negligible compared to the envelope part. Therefore, we neglect in the following the second part of Eq. (8) and thus the orbital contribution to the dipole matrix elements.

In analogy to the bulk systems, a separation of the orbital α and spin part σ is prohibited by the spin-orbit coupling. Additionally, due to band mixing effects, even the total angular momentum is not a good quantum number any more for the QD single-particle states so that the corresponding selection rules are no longer applicable. Any treatment of many-body effects in QDs based on these selection rules will yield inaccurate predictions of level degeneracies because the band mixing characteristics of zero-dimensional structures are ignored. However, the selection rules can always be analyzed on grounds of symmetry considerations. We point to Ref. 40 for a detailed discussion on this subject.

An often-discussed quantity in QD systems with a zincblende structure is the so-called *light-polarization anisotropy* λ. The light-polarization anisotropy is defined as the ratio of the absorption for light polarized along the $[1\bar{1}0]$ and $[110]$ axes[41]

$$\lambda = \frac{P_{[110]}}{P_{[1\bar{1}0]}} = \frac{|\langle \psi_1^e | r_{[110]} | \psi_1^h \rangle|^2}{|\langle \psi_1^e | r_{[1\bar{1}0]} | \psi_1^h \rangle|^2}. \quad (9)$$

As discussed in Ref. 41 for InAs QDs, the polarization anisotropy λ can deviate from unity for three different reasons: (i) The geometric dimensions of the QD are different along the $[110]$ and $[1\bar{1}0]$ directions. (ii) The underlying zincblende structure makes the $[110]$ and $[1\bar{1}0]$ directions inequivalent. (iii) A piezoelectric field breaks the symmetry. As discussed in Sec. II C, we neglect the piezoelectric field. Consequently, in a square-based pyramid, where the geometric factor does not contribute, a continuum-based approach such as a $\mathbf{k}\cdot\mathbf{p}$ model or an EBOM approximation neglecting piezoelectricity produces $\lambda = 1$. This is because these approaches neglect the atomistic details, except for small asymmetry effects that are introduced subsequently by an atomistic strain field.[42] It treats the square-based pyramid as having C_{4v} symmetry and therefore the $[110]$ and $[1\bar{1}0]$ directions as equivalent. For this reason, such an approach can only account for the geometrical factor. In a fully atomistic approach, such as a microscopic TB model or a pseudopotential calculation, both contributions are naturally included. Therefore, even in a square-based pyramidal QD, one could expect deviations from unity.

TABLE I. Comparison of level spacings calculated from the EBOM and the ETBM approaches.

	Electrons	
	EBOM	ETBM
Δ_{e_1,e_2} (meV)	136.5	128.6
Δ_{e_2,e_3} (meV)	0	0.2
	Holes	
	EBOM	ETBM
Δ_{h_1,h_2} (meV)	5.6	6.2
Δ_{h_2,h_3} (meV)	6.2	6.0
E_g (meV)	3670.9	3688.7

III. ELECTRONIC AND OPTICAL PROPERTIES OF CUBIC GaN/AlN QUANTUM DOTS

In the following section, we discuss the single-particle states and energies of the first three bound electron and hole states of a truncated pyramidal GaN/AlN QD. Section III B is dedicated to the excitonic absorption spectrum and the polarization anisotropy in these systems.

A. Single-particle states and energies

The calculated energy splittings $\Delta_{\alpha,\beta}$ between the different electronic levels are summarized in Table I, while Fig. 1 depicts the QD geometry and the modulus squared of the electron and hole wave functions for the first three bound states. Comparing the results of the two approaches, the calculated bound electron and hole states are very similar with respect to their symmetry properties as well as to their energies.

As it can be seen from Table I, the ETBM results for the energy splittings Δ_{e_i,e_j} of the different shells agree within 8 meV (5.8%) with the corresponding quantities of the EBOM.

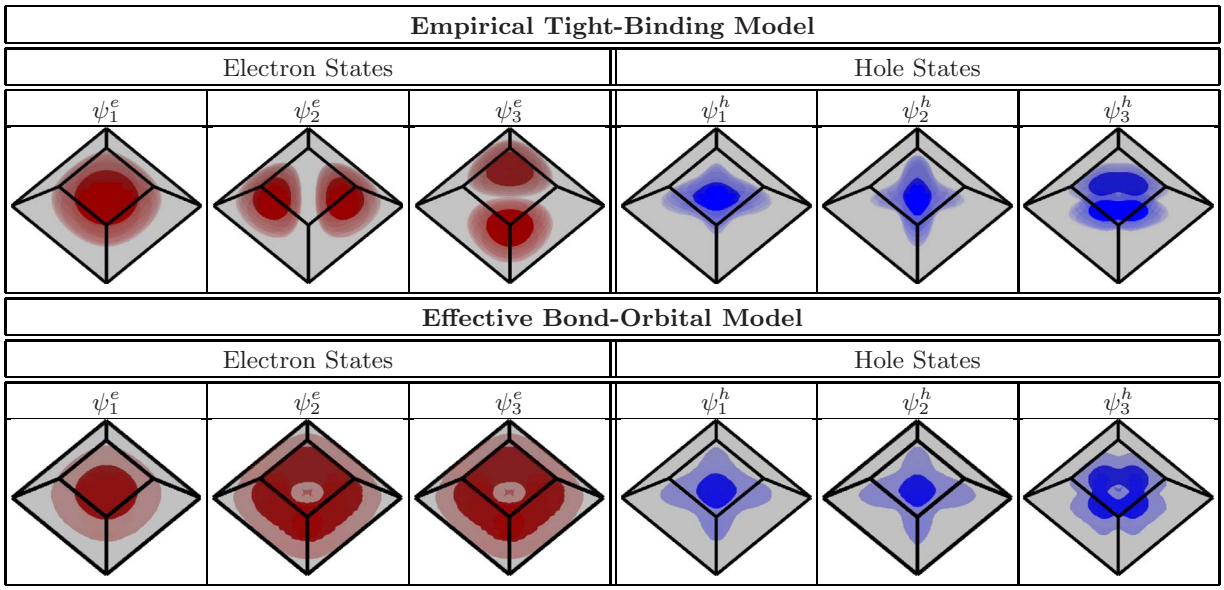

FIG. 1. (Color online) Isosurfaces of the first three modulus squared electron and hole wave functions for truncated pyramidal GaN/AlN QD (h=1.75 nm, b=7 nm) calculated with the empirical tight-binding model and the effective bond-orbital model. The light and dark surfaces correspond to 0.1 and 0.5 of the maximum probability density, respectively.

In case of the hole states, the results agree within 0.6 meV (10.8%). The single-particle energy gap calculated from the ETBM matches the EBOM results within 18 meV (0.5%).

While the calculated EBOM and ETBM bulk band structures are in excellent agreement around the Γ point, we find deviations around the X point.[32] Although the lateral dimension of the QD structure is large, it is very thin (≈2 nm) along the growth direction. Thus, the confined hole and electron states might include contributions with larger k_z, which result in different energies for these states. Therefore, slight deviations might arise from this issue.

Looking at the electron wave functions themselves, these states can be classified according to their nodal structure as s-like (ψ_1^e) and p-like (ψ_2^e, ψ_3^e) wave functions. Since the EBOM does not resolve the underlying zincblende structure, an unstrained, square-based (truncated) pyramidal GaN/AlN QD is modeled with a C_{4v} symmetry. Consequently, the states ψ_2^e and ψ_3^e are degenerate in the EBOM approach and can be described using linear combinations of the form $p_\pm = (1/\sqrt{2})(p_x \pm ip_y)$. In a microscopic description such as the ETBM, the resulting degeneracy is lifted and a splitting occurs as a consequence of the reduction of the C_{4v} to a C_{2v} zincblende symmetry. This symmetry reduction also gives rise to a larger splitting of the first two hole states ψ_1^h and ψ_2^h (cf. Table I). This analysis is confirmed by a closer inspection of these two groups. Since the C_{2v} group is Abelian, each irreducible representation is one dimensional.[43] Therefore, neglecting the spin, each state must be nondegenerate. In contrast to the C_{2v} group, the group C_{4v} is *non*-Abelian. In this case, we have four one-dimensional representations and one two-dimensional representation.[44] In conclusion, one would expect degenerate states in systems with a C_{4v} symmetry but not in systems with an overall symmetry group of C_{2v}. Note that this analysis neglects the influence of the spin-orbit interaction. Taking spin-orbit coupling into account, one has to consider the double groups, with the same single group representations and the additional degeneracies due to time-reversal symmetry.[45] In our calculations, the spin-orbit coupling is included, but it produces no significant effects for the electron states.

Due to band mixing effects, the hole states cannot be easily classified according to their nodal structure. Consequently, the selection rules will also be modified since the band mixing effects prevent a strict classification in terms of total angular-momentum selection rules. Therefore, the use of a multiband approach is crucial. In contrast to the EBOM approach, the first two hole states in the ETBM reveal a strong spatial anisotropy along the $[1\bar{1}0]$ and [110] directions, respectively. The same is true for the first two excited electron states ψ_2^e and ψ_3^e. This anisotropy again reflects the C_{2v} symmetry of the system under consideration. As discussed in detail in Ref. 32, the first two hole states are split by about 6 meV due to the underlying zincblende structure and the spin-orbit coupling. These two effects will strongly modify the optical properties of a truncated pyramidal GaN/AlN QD with a zincblende structure, as we will discuss in detail in the following section.

B. Excitonic absorption spectra

Starting from the calculated single-particle wave functions, the dipole and Coulomb matrix elements are obtained following Sec. II D. The calculation of excitonic absorption spectra in this section can directly be performed starting from the many-particle Hamiltonian in second quantization as given in Sec. II D. For the localized states, CI calculations are performed.[23] Since we are only interested here in comparing the resulting spectra of the EBOM and the ETBM, only the first three bound states for electrons and holes are included in the calculation. The excitonic absorption spectra are calculated using Fermi's golden rule. The calculation of the optical spectra is described in detail in Refs. 23 and 40.

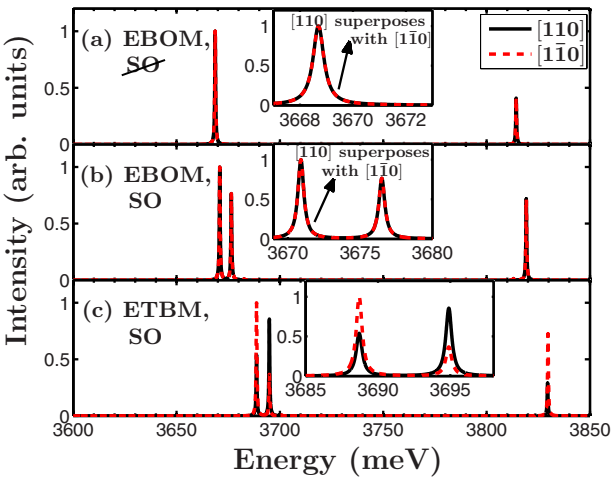

FIG. 2. (Color online) Excitonic absorption spectrum of a truncated pyramidal GaN for different light polarizations. The EBOM results without the spin-orbit coupling are shown in (a) while (b) shows the spectrum when including the spin-orbit coupling. The excitonic absorption spectrum calculated from the ETBM wave functions under the influence of the spin-orbit coupling is displayed in (c). All calculations are performed in the absence of the Coulomb interaction.

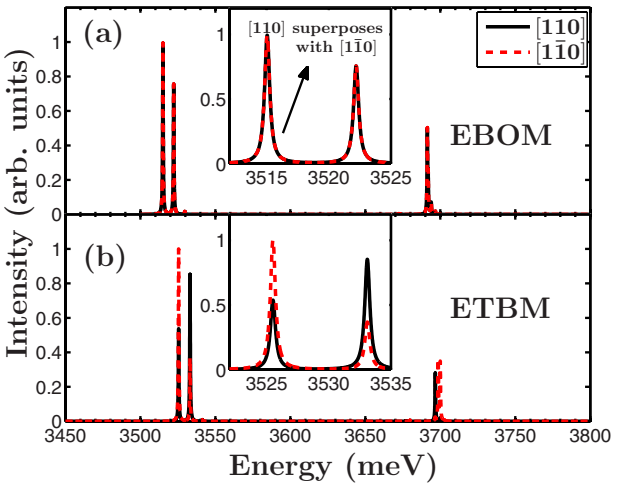

FIG. 3. (Color online) Excitonic absorption spectrum of a truncated pyramidal GaN for different light polarizations. (a) EBOM spectrum with Coulomb interaction and spin-orbit coupling. (b) ETBM spectrum with Coulomb interaction and spin-orbit coupling.

To study the influence of the different contributions in detail, we proceed in the following way. In a first step, we neglect the Coulomb interaction between the carriers. Furthermore, to study the possible influence of the weak spin-orbit coupling, we artificially switch-off this contribution. The spin-orbit coupling has been commonly neglected in III-nitride QD systems.[8,9,25–29] Figure 2(a) shows the excitonic absorption spectra of the EBOM without spin-orbit coupling, while Fig. 2(b) displays the spectrum in the presence of the spin-orbit interaction. The excitonic absorption spectrum calculated from the ETBM approach including spin-orbit coupling is shown in Fig. 2(c).

The spectrum of the QD is calculated for different light polarizations [$\mathbf{e} \sim (x, \pm y, 0)$]. The absorption lines in each spectrum correspond to the excitation of an exciton in the QD. Without Coulomb interaction, the two peaks on the low-energy side correspond to transitions where the electron is in the ground state ψ_1^e and the hole in the states ψ_1^h and ψ_2^h ($\psi_1^e - \psi_1^h; \psi_1^e - \psi_2^h$), respectively. The two bright lines for the polarizations [1$\bar{1}$0] and [110] on the high-energy side correspond to the transitions $\psi_2^e - \psi_3^h$ and $\psi_3^e - \psi_3^h$.

When comparing the results in the absence [cf. Fig. 2(a)] and in the presence [cf. Fig. 2(b)] of the spin-orbit coupling, the transition energies are only slightly affected by this contribution. The ground-state transition without spin-orbit interaction matches the result of the calculation including spin-orbit coupling within 2.2 meV. The main drawback of this approximation is the introduction of an artificial degeneracy in the hole spectrum as discussed in the previous section. Without the spin-orbit coupling, ψ_1^h and ψ_2^h are degenerate and therefore the calculation predicts a fourfold degenerate hole ground state in contrast to a twofold degenerate ground state when taking spin-orbit coupling into account. A similar behavior is observed in InN/GaN QDs with a wurtzite structure.[46] Therefore, in the absence of the spin-orbit interaction and neglecting the atomistic structure of the underlying crystal lattice, we observe only one peak on the low-energy side although there should in fact be two lines. Since the states ψ_1^h and ψ_2^h are split by about 6 meV due to the spin-orbit coupling, these lines are energetically separated by this value.

When comparing the results from the ETBM and the EBOM, the overall agreement in the transition energies is very good, e.g., the ground-state transition agrees within 18 meV. Furthermore, in both approaches, the calculations for $\mathbf{e} \sim (0,0,z)$ (not shown) reveal that there is a strong anisotropy between the [001] and the in-plane polarization directions.

In contrast to the EBOM approach, the ETBM predicts an anisotropy between [1$\bar{1}$0] and [110] directions [cf. Fig. 2(c)]. This anisotropy reflects the C_{2v} symmetry of the single-particle wave functions in case of the atomistic approach. The magnitudes of the oscillator strength for the [110] and [1$\bar{1}$0] directions follow from the orientations of the single-particle states displayed in Fig. 1. For example, the electron ground state is nearly isotropic. Due to the underlying zincblende structure, the hole ground state in the framework of the ETBM is aligned along the [1$\bar{1}$0] direction. Therefore the transition $\psi_1^e - \psi_1^h$ is favored by the [1$\bar{1}$0] polarization, while in case of the EBOM approach, the first two hole states are fairly symmetric and no polarization anisotropy is observed.

Including the Coulomb interaction (cf. Fig. 3), the absorption lines shift to lower energies due to the attractive interaction between electron and hole. According to the CI calculation, the two lines on the low-energy side are dominated by contributions where the electron is in the state ψ_1^e and the hole in the states ψ_1^h and ψ_2^h, respectively.

The ratios of the dipole matrix elements for light polarized along the [1$\bar{1}$0] and [110] directions are calculated from Eq. (9). In case of the $\psi_1^e - \psi_1^h$ transition, we find a polariza-

tion anisotropy ratio of $\lambda=0.54$ for this truncated pyramidal GaN QD. Again, the magnitude of the ratio reflects the orientation of the single-particle states displayed in Fig. 1.

Therefore, even without strain and piezoelectricity, we observe a strong polarization anisotropy in the framework of a fully atomistic approach. This result is in strong contrast to the results of symmetric QDs with a wurtzite structure grown along the c axis. In such a system, no polarization anisotropy is observed.[46,47] Only if the QD is elongated along one direction, the polarization anisotropy is introduced due to the shape breaking the symmetry of the x-y plane, but in general we expect symmetric emission from c-axis QDs. The strongly linear polarization of the excitonic transitions in cubic GaN/AlN QDs might be of significant potential benefit for a range of applications, e.g., back lighting liquid crystal displays.

A strong polarization anisotropy in cubic GaN/AlN QDs has been measured recently in photoluminescence (PL) experiments.[24] Lagarde *et al.*[24] observed a significant PL linear polarization ($\approx 15\%$) when the excitation is linearly polarized. This is a clear signature of the partial linear polarization of the excitonic transitions along the [110] and $[1\bar{1}0]$ directions. To further confirm the results, the authors have measured the PL linear polarization as a function of the angle θ between the linear polarization of the excitation and the [110] and $[1\bar{1}0]$ directions.

To compare our calculations to the experimental data, we calculate the intensity of the excitonic ground-state transition as a function of the polarization vector $\mathbf{e}(\theta)$, where θ denotes the angle between the polarization vector $\mathbf{e}$ and the [110] axis. As reference, we use the intensity I^x of the ground-state transition with $\mathbf{e}(\theta=45°)$. Therefore, we define the degree of linear polarization P_{lin} as

$$P_{\mathrm{lin}}(\theta) = \frac{I^x - I(\theta)}{I(0°) + I(90°)}. \tag{10}$$

The calculated $P_{\mathrm{lin}}(\theta)$ from the ETBM approach (blue squares) and the EBOM approach (green diamonds) is shown in Fig. 4. Due to the C_{4v} symmetry of the combined system of QD geometry and underlying lattice in the framework of the EBOM, no linear polarization is observed, while in the ETBM results, the degree of the linear polarization is given by $P_{\mathrm{lin}}(\phi) \propto \cos(2\theta)$, which is characteristic for a system with C_{2v} symmetry.[48] Therefore, the ETBM results are in very good agreement with the experimental data. Furthermore, the analysis of the optical spectra clearly shows the fingerprints of the electronic structure of the nanostructure.

In conclusion, our investigations reveal that a large part of the polarization anisotropy λ can already be explained by a square-based (truncated) pyramidal QD without piezoelectricity and an atomistic strain field when using a fully atomistic approach. In other words, even without a deformation of the pyramid, a microscopic approach might yield a distinct polarization anisotropy λ. Therefore, the geometric anisotropy of a QD might not be reliably deduced using $\mathbf{k}\cdot\mathbf{p}$ calculations to fit the measured polarization anisotropy, as suggested by Yang *et al.*,[49] since continuum-based simulations lack the correct atomistic symmetries. This comparison emphasizes the importance of an atomistic simulation for a detailed description of the optical properties of semiconductor QDs. Of course, when including additional effects, such as an atomistic strain field as well as piezoelectricity, the EBOM will also yield a polarization anisotropy. Furthermore, for large systems, the microscopic structure of the system will be of minor significance. For smaller height-to-base-length ratios, the influence of larger k_z might grow, thus requiring a suitable fit of the bulk band structure throughout the Brillouin zone. Therefore, the importance of the underlying crystal structure in comparison to other effects (strain, piezoelectricity) will strongly depend on the system under consideration and has to be checked carefully.

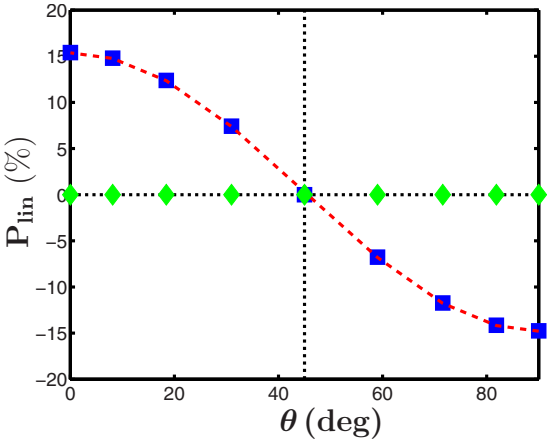

FIG. 4. (Color online) Linear polarization as a function of the angle θ between the polarization vector $\mathbf{e}$ and the [110] direction. The ETBM result is indicated by the blue squares, while EBOM result is given by the green diamonds.

IV. CONCLUSION

In this paper, we have studied the electronic and the optical properties of truncated pyramidal GaN/AlN QDs with a zincblende structure. In summary, we have compared the results of two slightly different tight-binding approaches to model QDs, namely, the atomistic ETBM and the EBOM, with a slightly lower, not atomistic but only lattice site resolution. Concerning the eigenstates and eigenenergies, the results obtained within the two methods essentially agree qualitatively and quantitatively, besides a small energetic shift. On one hand, small discrepancies between the ETBM energies and the experimental values for larger $\mathbf{k}$ might play a role. On the other hand, deviations between the microscopic ETBM and the EBOM are found to be related to the symmetry of the underlying crystal structure which is described correctly in the microscopic approach. This symmetry and the inclusion of the weak spin-orbit coupling leads, for instance, to a splitting of the p-like electron states and the first two hole states in case of a truncated pyramidal QD.

Dipole and Coulomb matrix elements have been calculated from these single-particle wave functions and serve as an input for configuration-interaction calculations. The theory has been applied to the evaluation of the excitonic absorption spectrum. For the calculated transition energies,

we find a very good agreement between the ETBM and EBOM results. Furthermore, we have demonstrated that the inclusion of the spin-orbit coupling is required to avoid artificial degeneracies in the hole spectrum, especially for the hole ground state. The EBOM cannot reproduce certain fine structures, which are obtained within the ETBM, for instance, that the lowest interband transition has a very different intensity along the [110] and $[1\bar{1}0]$ directions. This anisotropy exists even in the absence of strain and piezoelectricity, reflecting both the underlying C_{2v} symmetry of the QD system and the band mixing. Such an anisotropy is absent in the EBOM for square-based pyramidal QDs with a zincblende structure when neglecting contributions from an atomistic strain field and piezoelectric contributions, respectively. As the correct symmetry is taken into account in the ETBM, a polarization anisotropy, which has recently been observed experimentally,[24] can be reproduced within the ETBM.

ACKNOWLEDGMENTS

The authors would like to thank Eoin P. O'Reilly, Stefan Schumacher, Paul Gartner, and Jan-Peter Richters for fruitful discussions. This work has been supported by the Deutsche Forschungsgemeinschaft (research group "Physics of nitride-based, nanostructured, light-emitting devices," Project No. Cz 31/14-3). S.S. was further supported by the Humboldt Stiftung, the IRCSET Embark Initiative, and Science Foundation Ireland. We also acknowledge a grant for CPU time from the NIC at the Forschungszentrum Jülich and from the Norddeutscher Verbund für Hoch- und Höchstleistungsrechnen (HLRN).

[1] S. Nakamura, T. Mukai, and M. Senoh, Appl. Phys. Lett. **64**, 1687 (1994).
[2] C. H. Qiu, W. Melton, M. W. Leksono, J. I. Pankove, B. P. Keller, and S. P. DenBaars, Appl. Phys. Lett. **69**, 1282 (1996).
[3] H. Morkoc, S. Strite, G. B. Gao, M. E. Lin, B. Sverdlov, and M. Burns, J. Appl. Phys. **76**, 1363 (1994).
[4] T. Uenoyama, Phys. Rev. B **51**, 10228 (1995).
[5] F. Widmann, J. Simon, B. Daudin, G. Feuillet, J. L. Rouvière, N. T. Pelekanos, and G. Fishman, Phys. Rev. B **58**, R15989 (1998).
[6] J. Simon, N. T. Pelekanos, C. Adelmann, E. Martinez-Guerrero, R. Andre, B. Daudin, L. S. Dang, and H. Mariette, Phys. Rev. B **68**, 035312 (2003).
[7] S. V. Novikov, N. M. Stanton, R. P. Campion, R. D. Morris, H. L. Geen, C. T. Foxon, and A. J. Kent, Semicond. Sci. Technol. **23**, 015018 (2008).
[8] S. Schulz, S. Schumacher, and G. Czycholl, Phys. Rev. B **73**, 245327 (2006).
[9] A. D. Andreev and E. P. O'Reilly, Phys. Rev. B **62**, 15851 (2000).
[10] S. Founta, F. Rol, E. Bellet-Amalric, J. Bleuse, B. Daudin, B. Gayral, H. Mariette, and C. Moisson, Appl. Phys. Lett. **86**, 171901 (2005).
[11] S. Founta, F. Rol, E. Bellet-Amalric, E. Sarigiannidou, B. Gayral, C. Moisson, H. Mariette, and B. Daudin, Phys. Status Solidi B **243**, 3968 (2006).
[12] S. Founta *et al.*, J. Appl. Phys. **101**, 063541 (2007).
[13] S. Schulz, A. Berube, and E. P. O'Reilly, Phys. Rev. B **79**, 081401(R) (2009).
[14] H. Yang, L. X. Zheng, J. B. Li, X. J. Wang, D. P. Xu, Y. T. Wang, X. W. Hu, and P. D. Han, Appl. Phys. Lett. **74**, 2498 (1999).
[15] M. A. Moram, S. V. Novikov, A. J. Kent, C. Norenberg, C. T. Foxon, and C. J. Humphreys, J. Cryst. Growth **310**, 2746 (2008).
[16] E. Martinez-Guerrero, C. Adelmann, F. Chabuel, J. Simon, N. T. Pelekanos, G. Mula, B. Daudin, G. Feuillet, and H. Mariette, Appl. Phys. Lett. **77**, 809 (2000).
[17] C. Adelmann *et al.*, Mater. Sci. Eng., B **82**, 212 (2001).
[18] N. Gogneau *et al.*, Phys. Status Solidi C **1**, 1445 (2004).
[19] B. Daudin *et al.*, Jpn. J. Appl. Phys. **40**, 1892 (2001).
[20] J. P. Garayt *et al.*, Physica E (Amsterdam) **26**, 203 (2005).
[21] M. Bayer, O. Stern, P. Hawrylak, S. Fafard, and A. Forchel, Nature (London) **405**, 923 (2000).
[22] A. J. Williamson, A. Franceschetti, and A. Zunger, Europhys. Lett. **53**, 59 (2001).
[23] N. Baer, P. Gartner, and F. Jahnke, Eur. Phys. J. B **42**, 231 (2004).
[24] D. Lagarde, A. Balocchi, H. Carrère, P. Renucci, T. Amand, S. Founta, H. Mariette, and X. Marie, Microelectron. J. **40**, 328 (2009).
[25] V. A. Fonoberov and A. A. Baladin, J. Appl. Phys. **94**, 7178 (2003).
[26] A. D. Andreev and E. P. O'Reilly, Appl. Phys. Lett. **79**, 521 (2001).
[27] T. Saito and Y. Arakawa, Physica E (Amsterdam) **15**, 169 (2002).
[28] T. Saito and Y. Arakawa, Phys. Status Solidi C **0**, 1169 (2003).
[29] N. Baer, S. Schulz, S. Schumacher, P. Gartner, G. Czycholl, and F. Jahnke, Appl. Phys. Lett. **87**, 231114 (2005).
[30] L. W. Wang, A. J. Williamson, A. Zunger, H. Jiang, and J. Singh, Appl. Phys. Lett. **76**, 339 (2000).
[31] S. Schulz and G. Czycholl, Phys. Rev. B **72**, 165317 (2005).
[32] O. Marquardt, D. Mourad, S. Schulz, T. Hickel, G. Czycholl, and J. Neugebauer, Phys. Rev. B **78**, 235302 (2008).
[33] D. J. Chadi, Phys. Rev. B **16**, 790 (1977).
[34] J. P. Loehr, Phys. Rev. B **50**, 5429 (1994).
[35] D. Fritsch, H. Schmidt, and M. Grundmann, Phys. Rev. B **67**, 235205 (2003).
[36] I. Schnell, G. Czycholl, and R. C. Albers, Phys. Rev. B **65**, 075103 (2002).
[37] G. W. Bryant and W. Jaskolski, Phys. Rev. B **67**, 205320 (2003).
[38] K. Leung and K. B. Whaley, Phys. Rev. B **56**, 7455 (1997).
[39] S. Lee, J. Kim, L. Jönsson, J. W. Wilkins, G. W. Bryant, and G. Klimeck, Phys. Rev. B **66**, 235307 (2002).
[40] N. Baer, S. Schulz, P. Gartner, S. Schumacher, G. Czycholl, and F. Jahnke, Phys. Rev. B **76**, 075310 (2007).
[41] L. W. Wang, J. Kim, and A. Zunger, Phys. Rev. B **59**, 5678 (1999).
[42] G. Bester and A. Zunger, Phys. Rev. B **71**, 045318 (2005).

[43] M. J. Lax, *Symmetry Principles in Solid State and Molecular Physics* (Wiley, New York, 1974).
[44] J. F. Cornwell, *Group Theory and Electronic Energy Bands in Solids* (North-Holland Pubishing Company, Amsterdam, 1969).
[45] H. W. Streitwolf, *Group Theory in Solid-State Physics* (Macdonald, London, 1971).
[46] S. Schulz, S. Schumacher, and G. Czycholl, Eur. Phys. J. B **64**, 51 (2008).
[47] M. Winkelnkemper, R. Seguin, S. Rodt, A. Schliwa, L. Reißmann, A. Strittmatter, A. Hoffmann, and D. Bimberg, J. Appl. Phys. **101**, 113708 (2007).
[48] A. V. Koudinov, N. S. Averkiev, Y. G. Kusrayev, B. R. Namozov, B. P. Zakharchenya, D. Wolverson, J. J. Davies, T. Wojtowicz, G. Karczewski, and J. Kossut, Phys. Rev. B **74**, 195338 (2006).
[49] W. Yang, H. Lee, T. J. Johnson, P. C. Sercel, and A. G. Norman, Phys. Rev. B **61**, 2784 (2000).